

Crawling and Jumping by a Deformable Robot

Yuuta Sugiyama

Shinichi Hirai

Department of Robotics, Ritsumeikan University

Kusatsu, Shiga 525-8577, Japan

E-mail: hirai@se.ritsumei.ac.jp

corresponding author: Shinichi Hirai

Abstract

We describe crawling and jumping by a soft robot. Locomotion over rough terrain has been achieved mainly by rigid body systems including crawlers and leg mechanisms. This paper presents an alternative method, one that employs deformation. First, we describe the principle of crawling and jumping as performed through deformation of a robot body. Second, in a physical simulation, we investigate the feasibility of the approach. Next, we show experimentally that a prototype of a circular soft robot can crawl and jump. Finally, we describe crawling and jumping performed by a spherical deformable robot.

Keywords: deformation, locomotion, crawl, jump

1 Introduction

Rough terrain locomotion has mainly relied on rigid body systems, such as crawlers and leg mechanisms. This paper presents an alternative approach that uses deformation.

Snake-like robots have been studied for the past decade to improve their locomotion performance over rough terrain (Hirose and Morishima 1990; Hirose 1993). Hopping legged robots that can perform dynamic maneuvers over the ground are also being studied (Raibert 1986; Hodgins and Raibert 1990; Higashimori et al. 2005). But, being heavy, they are not good at uprighting themselves when they overturn and they pose a risk of injury or damage should they crash into people or objects. Robots capable of recovering from overturning have recently been developed (Hale et al. 2000; Saranli et al. 2001; Yim et al. 2004), but they are usually complicated. Thus, light and simple robots that can traverse rough terrain are required, and to make them, an alternative method of locomotion is required. Recent studies on soft actuators such as shape memory alloy (SMA) wires and polymer or gel actuators have yielded impressive results (Pelrine et al. 2000; Ashley 2003; Hirai et al. 2003; Choi et al. 2003; Selden et al. 2004). Robots with these actuators can be soft and light. Unfortunately, soft actuators still have drawbacks. They typically cannot generate large impulse, and those that can require a wet environment or a high driving voltage of over 1,000 V, making it difficult to build self-supporting

robots. To overcome this problem, we employ soft actuators to controllably deform a robot body, enabling it to crawl and jump on rough terrain. Self-deformation of the robot body generates the spatial gradient of the gravitational potential energy of the robot crawling along the ground. By charging the elastic potential energy in the robot's deformable body and releasing it rapidly, the robot generates enough impulse to make it jump. Crawling and jumping by deformation enables the robot to be used over terrain too rough for rigid body robots. Additionally, soft-body deformation reduces the risk of injury should the body collides with humans.

Soft materials have been used for robot systems. Flexible manipulators with bendable links have been studied extensively to control the position and posture of their end point (Book and Majette 1983; Ge et al. 1996; Matsuno et al. 2002). But, flexibility of the links is regarded as a hindrance to accurate positioning. Soft-fingered hands have been studied for stable grasping and manipulation (Shimoga and Goldenberg 1996; Xydias and Kao 1999; Nguyen and Arimoto 2001). Soft fingers provide contact force regulation in grasping and tangential force generation during manipulation, which yield secure and simple grasping and manipulation. In these studies, deformable objects are passive: they deform in response to external forces.

In this paper, we investigate experimentally the feasibility of locomotion of a robot body through deformation. We propose a deformable robot that can crawl and jump, and describe its performance in simulation and in practice. Soft-body robots driven by gel actuators (Otake et al. 2002) and an underwater vehicle driven by self-deformation (Chen et al. 2003) have been proposed. These mechanisms work in water. There is a Web site on computer simulation of virtual deformable robots (sodaplay), but it does not mention that robots were actually built. This paper represents the first attempt at using *active* deformation of a robot body for locomotion on the ground. First, we describe the principle of crawling and jumping as performed through deformation of a robot body. Second, in a physical simulation, we investigate the feasibility of the approach. Next, we build a prototype of a circular soft robot and demonstrate that it can crawl and jump. Finally, we describe crawling and jumping as performed by a prototype of a spherical deformable robot.

2 Principle of Crawling and Jumping by Deformation

Suppose a robot is stable on the ground, as illustrated in Figure 1-(a). The gravitational potential energy of the robot is at its minimum, i.e., the gradient of the energy with respect to space is equal to zero. Self-deformation of the robot body changes the gradient of the gravitational potential energy; a moment is generated due to the gravitational force around the area of contact between the robot and the ground. This moment causes the robot to move along the ground. If the robot deforms from the stable shape into the unstable shape shown in Figure 1-(b), it rotates clockwise and moves towards the right until it takes on the stable shape shown in Figure 1-(c). Repeated deformation of the robot body, which can be generated by actuators, enables a continuous crawling motion along the ground. Thus, the proposed crawling approach relies on the change in gravitational potential energy caused by the deformation of the robot body.

Deformation allows elastic potential energy to be stored, which, if released rapidly enough, can generate an impulse large enough to make the robot jump. Now, suppose the robot changes from a stable shape into one with high potential energy, as illustrated in Figure 1-(d). If this

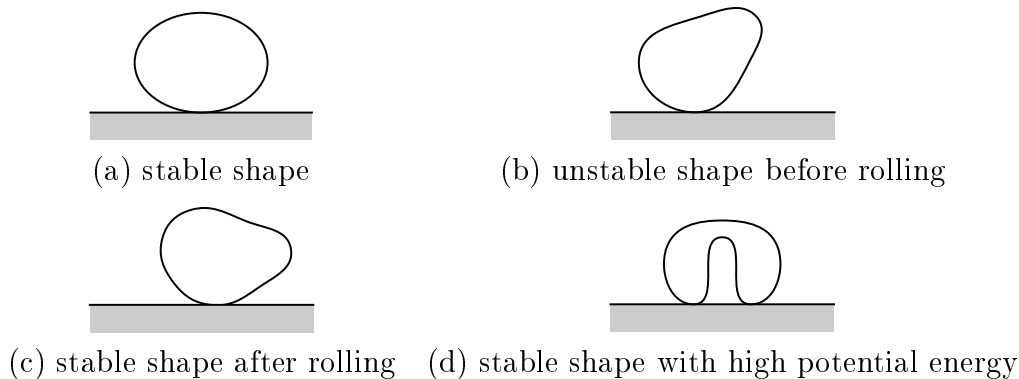


Figure 1: Principle of crawling and jumping

potential energy is released rapidly enough, the robot will jump. The high-energy shape shown in Figure 1-(d) changes, with a small disturbance, into the stable shape shown in Figure 1-(a), generating the impulse required for the jump. Thus, the jumping action comes from charge and rapid release of elastic potential energy. That is, the robot body functions as a *mechanical capacitor*. Actuators inside the robot body can be used to store elastic energy. The speed of deformation of the robot body is mainly governed by the speed of actuators during charging of the elastic energy, and by viscoelasticity of the body during the release of the energy. Thus, the robot body deforms much faster during the release of the elastic energy than during the energy charging. This implies that the robot body has more linear momentum during the release of the potential energy, generating an impulse large enough for the robot jump. Such charge and release of elastic energy has been used to capture objects (Kaneko et al. 2003). Insects are known to exploit the charge and release of elastic energy for jumping (Rothschild et al. 1986).

3 Feasibility Study through Physical Simulation

In this section, we use a physical simulation to assess the feasibility of a deformable robot crawling and jumping. As mentioned in the previous section, crawling and jumping can be performed using the gravitational potential energy and the elastic energy associated with deformation. Let us verify this approach through a physical simulation before we move on to a prototype of a deformable robot. We apply particle-based modeling to simulate the behavior of a deformable robot. A deformable robot is described by a set of particles connected by mechanical elements, which characterize the deformation of the robot. By solving a set of equations of motion for the particles, we can simulate the behavior of a deformable robot. All programs are written in C/C++ language and OpenGL is used for graphic display.

3.1 Modeling of circular elastic shell

Let us simulate the behavior of the circular soft robot illustrated in Figure 2. The robot consists of a circular elastic shell with a set of soft actuators inside, as shown in Figure 2-(a). The robot has eight SMA coils labeled A through H. An SMA coil is made by winding an SMA

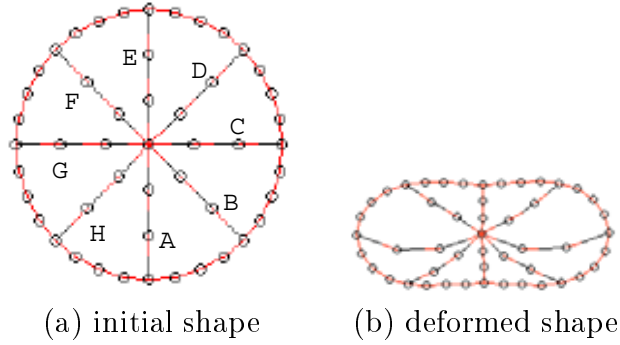


Figure 2: Circular soft robot

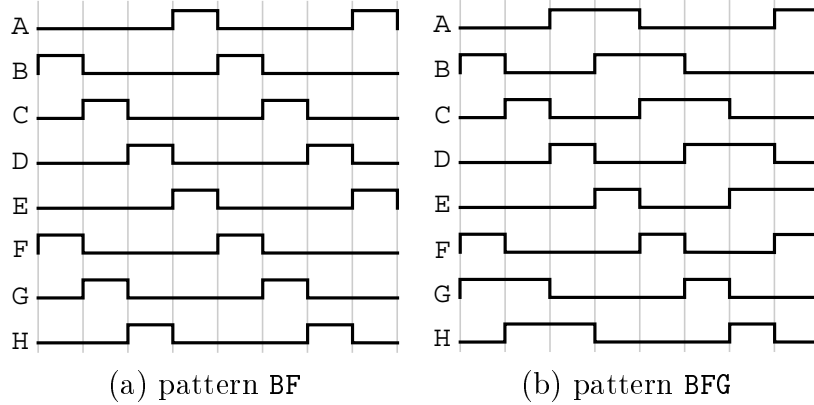


Figure 3: Voltage patterns applied to SMA coils

wire, enabling large and fast shrinkage. Shrinking the actuators deforms the robot body, i.e., the circular shell, as shown in Figure 2-(b). We apply open-loop PWM control to the coils. A periodic voltage pattern is applied to the set of SMA coils during crawling. As illustrated in Figure 3, periodic voltage patterns are denoted by the set of coils active during the first time-step. Figure 3-(a) illustrates pattern **BF**, where SMA coils B and F are activated during the first time-step, coils C and G during the second time-step, coils D and H during the third time-step, and so on. Figure 3-(b) illustrates pattern **BFG**, where SMA coils B, F, and G are activated during the first time-step and coils C, G, and H during the subsequent time-step.

The elastic shell of the robot is modeled as an elastic object, while the actuators are modeled as rheological objects (Kimura et al. 2003), so as to be able to describe the inelastic nature of the SMA coils and polymer gel actuators. We can specify the contraction rate, maximum contraction, and maximum generated force of an SMA coil using a three-element model with a slider.

The extension of an elastic shell can be described by a Voigt model, while its bend can be modeled as an elastic element. The Voigt model for an extension is a parallel connection between an elastic element k_{body} and a viscous element b_{body} . The elastic element for bend deformation is denoted by k_{bend} . Let P_i and P_j be two neighboring particles on a circular body, as illustrated in Figure 4. Let \mathbf{x}_i and \mathbf{x}_j be the position vectors of the two particles. Introducing displacement

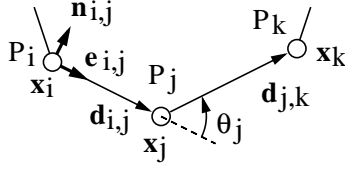


Figure 4: Model of the circular elastic shell

vector $\mathbf{d}_{i,j} = \mathbf{x}_j - \mathbf{x}_i$, the distance between the two neighboring particles and its time rate of change are given by

$$d_{i,j} = \|\mathbf{d}_{i,j}\|, \quad \dot{d}_{i,j} = \dot{\mathbf{d}}_{i,j} \cdot \mathbf{e}_{i,j},$$

where $\mathbf{e}_{i,j} = \mathbf{d}_{i,j}/d_{i,j}$ represents the unit vector from particle P_i to P_j . According to the Voigt model, the force generated between the two particles is:

$$\mathbf{f}_{i,j}^{\text{body}} = \left\{ k_{\text{body}}(d_{i,j} - d_{i,j}^{\text{init}}) + b_{\text{body}}\dot{d}_{i,j} \right\} \mathbf{e}_{i,j},$$

where $d_{i,j}^{\text{init}}$ denotes the natural length of the model. The force $\mathbf{f}_{i,j}^{\text{body}}$ is exerted on particle P_i , while the reaction force $-\mathbf{f}_{i,j}^{\text{body}}$ is exerted on particle P_j . Let θ_j denote the angle by which the circular body is bent at particle P_j , as illustrated in Figure 4. Let P_i and P_k be particles adjacent to P_j . Then, angle θ_j is given by

$$\theta_j = \arctan \left\{ \frac{\mathbf{d}_{i,j} \times \mathbf{d}_{j,k}}{\mathbf{d}_{i,j} \cdot \mathbf{d}_{j,k}} \right\}.$$

The elastic element corresponding to the bend deformation at particle P_j generates a moment given by $\tau_j^{\text{bend}} = -k_{\text{bend}}\theta_j$ around the particle. Let us introduce vector $\mathbf{n}_{i,j}$ so that $\mathbf{e}_{i,j}$ and $\mathbf{n}_{i,j}$ form a right-handed coordinate system, as illustrated in Figure 4. The moment is then converted into three equivalent forces, namely $(\tau_j^{\text{bend}}/d_{i,j})\mathbf{n}_{i,j} + (\tau_j^{\text{bend}}/d_{j,k})\mathbf{n}_{j,k}$, $-(\tau_j^{\text{bend}}/d_{i,j})\mathbf{n}_{i,j}$, and $-(\tau_j^{\text{bend}}/d_{j,k})\mathbf{n}_{j,k}$ acting, respectively, on particle P_j and its neighboring particles P_i and P_k .

As shown in Section 4, the elastic shell of the prototype of the circular soft robot is made of rubber. The circular shell is modeled as a series of 32 particles forming a circle. The rubber shell weighs 2.5 g, the mass of each particle being 0.078 g. In addition, we have experimentally identified model parameters for the circular rubber shell in advance: $k_{\text{body}} = 500 \text{ N/m}$, $b_{\text{body}} = 0.1 \text{ N/(m/s)}$, and $k_{\text{bend}} = 0.0015 \text{ Nm/rad}$.

3.2 Modeling of SMA coil

Let us first formulate the passive deformation of an SMA coil that deforms in response to an applied external force. SMA coils show both viscoelastic and plastic deformation properties, which suggests that their deformation can be modeled by a three-element model. Figure 5-(a) illustrates a three-element model, consisting of a Voigt element connected in serial to a viscous element. The elastic coefficient k and damping coefficient b characterize the Voigt element, while the viscous coefficient c characterizes the viscous element. Let x_v^{init} and x_d^{init} be the initial length

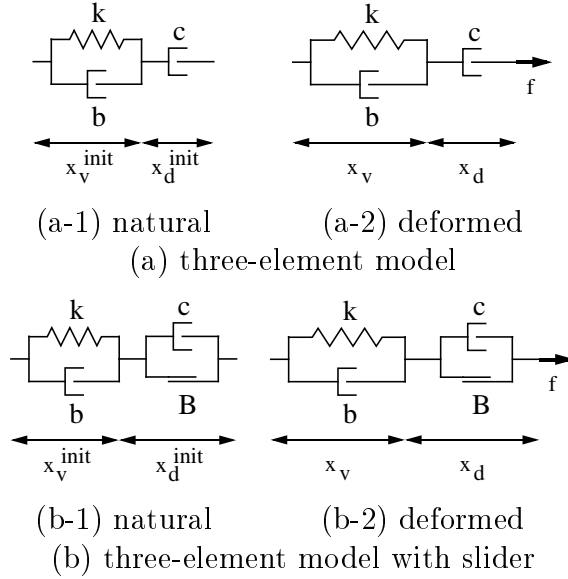


Figure 5: Model of SMA coils

of the Voigt element and the initial length of the viscous element, respectively. Let x be the length of the three-element model. Let x_v and x_d be the lengths of the Voigt element and the viscous element, respectively. The three-element model can be formulated as follows:

$$x = x_v + x_d, \quad (1)$$

$$f_{\text{pas}} = -k(x_v - x_v^{\text{init}}) - b\dot{x}_v, \quad (2)$$

$$f_{\text{pas}} = -c\dot{x}_d \quad (3)$$

where f_{pas} describes the passive force generated by the element. The initial length x_v^{init} determines the maximum contraction of an SMA coil.

A three-element model can extend until the external force is removed. To avoid such limitless extension, we employ a three-element model with a slider illustrated in Figure 5-(b). The slider is specified by force limit B . In a three-element model with a slider, eq.(3) is replaced by the following equation:

$$-c\dot{x}_d = \begin{cases} f_{\text{pas}} & \text{if } f \leq 0 \text{ or } Bx \leq f x_v^{\text{init}} \\ 0 & \text{otherwise} \end{cases} \quad (4)$$

where f stands for the resultant external force applied on the element. A viscous element with a slider stops extending when it reaches a length threshold determined by f and x_v^{init} , even though the external force may still be acting.

An SMA coil actively generates a force that is determined by the voltage applied to it. Let us next formulate this force. Let $V(t)$ be the voltage applied to the coil. We apply open-loop PWM to the generation of the force by the coil. That is, voltage $V(t)$ alternates between V and 0. Let $F(t)$ be the force actively generated by the SMA coil at time t . Let D_{on} be the contraction force rate of the coil and D_{off} its relaxation force rate. Let F_{max} be the maximum force that can be

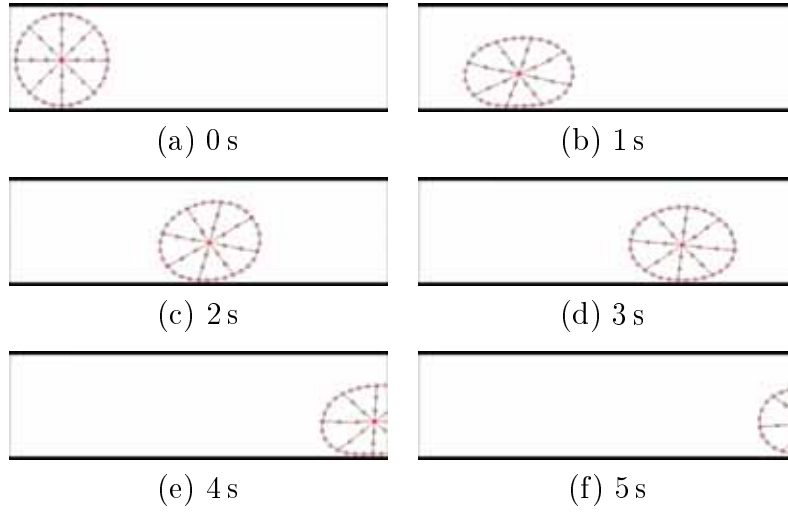


Figure 6: Simulation of a circular soft robot crawling

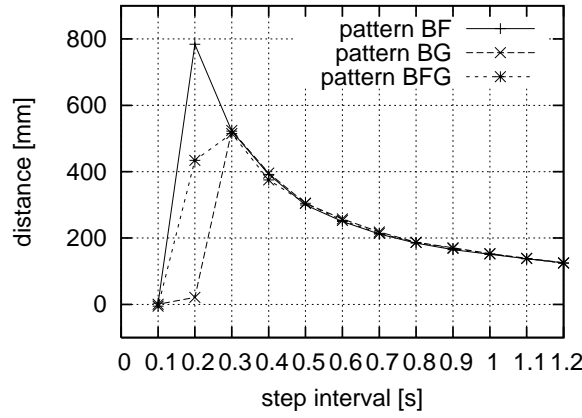


Figure 7: Comparison of pattern BF, BG, and BFG

generated by the coil. The force generated by the SMA coil can then be expressed as:

$$\frac{dF}{dt} = \begin{cases} D_{\text{on}} & V(t) = V \text{ and } F(t) < F_{\text{max}} \\ -D_{\text{off}} & V(t) = 0 \text{ and } F(t) > 0 \\ 0 & \text{otherwise} \end{cases} . \quad (5)$$

Integration of the above equation over the time interval $[0, t]$ yields the actively generated force at time t . Note that force $F(t)$ varies in the range $[0, F_{\text{max}}]$.

We used eight BMX100 SMA coils (Toki Corporation, Japan), as actuators, in a prototype of a circular soft robot. Each coil is described by a series of 4 particles. One end particle is involved in the circular elastic shell and the other end corresponds to the center particle. Together, the SMA coils weigh 1.1 g, of which 0.3 g is assigned to the center particle and 0.05g to each of the other 16 particles. In addition, we experimentally identified the model parameters to be used in eqs.(1)-(5): $k = 50 \text{ N/m}$, $b = 0.1 \text{ N/(m/s)}$, $c = 10 \text{ N/(m/s)}$, $B = 62.5 \text{ N}$, $D_{\text{on}} = D_{\text{off}} = 150 \text{ mN/s}$, and $F_{\text{max}} = 150 \text{ mN}$.

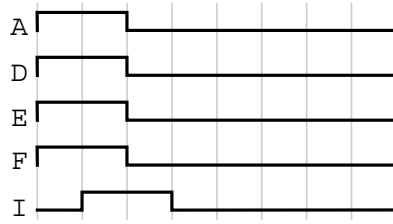


Figure 8: Voltage pattern for jumping

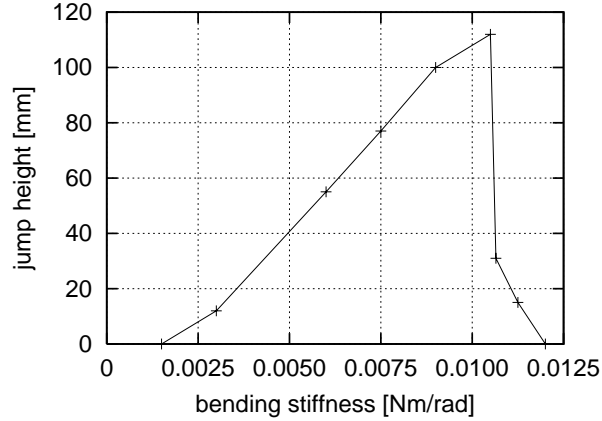


Figure 9: Simulated jump height

3.3 Simulation results

Figure 6 shows the simulation results for the crawling of a circular soft robot. A reaction force between a robot and a terrain can be described by a Voigt model and a Coulomb friction model. A normal reaction force, which is characterized by a Voigt model with elasticity $k_{\text{terrain}} = 1000 \text{ N/m}$ and viscosity $b_{\text{terrain}} = 1 \text{ N}/(\text{m/s})$, is applied to particles penetrating the terrain. Static or kinetic friction forces are applied to the penetrating particles, and their friction coefficients are 0.5 and 0.3 in the following simulations. A periodic voltage pattern is applied to one or more of the SMA coils during the crawl. In this simulation, pattern BF (see Figure 3-(a)) was used to activate the coils. The figure shows that a circular robot can crawl on a flat terrain by open-loop PWM control of eight SMA coils. Simulation also allows us to find a better voltage pattern. Figure 7 shows locomotion distances covered in 10 s using three voltage patterns, BF, BG, and BFG, at various step intervals. As shown in the figure, voltage pattern BF with a step interval of 0.2 s yields the best result among the simulated patterns.

For jumping, we attach an SMA coil labeled I between the end points of B and H on the circular shell in addition to the eight SMA coils. The voltage pattern illustrated in Figure 8 is applied to a set of SMA coils. The four SMA coils, A, D, E, and F, are activated before coil I. Thus, the robot deforms into the stable shape and potential energy is stored. The four coils are then released so that a single coil, I, keeps the robot deformed. Finally, upon release of coil I, the robot jumps. From the simulation, we find that the robot cannot jump when $k_{\text{bend}} = 0.0015 \text{ Nm/rad}$ and $F_{\text{max}} = 150 \text{ mN}$. This suggests that we have to increase the maximum force F_{max} and, at the

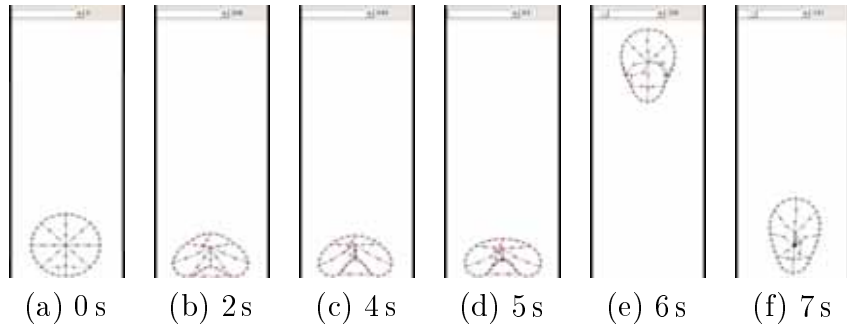


Figure 10: Simulation of a circular soft robot jumping

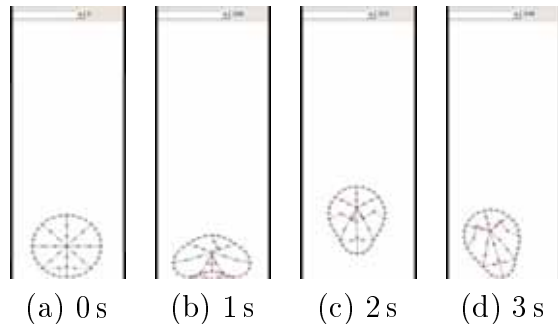


Figure 11: Simulation of a jump with large elastic coefficient for bending

same time, the bending stiffness k_{bend} . Let us increase the maximum force F_{max} from 150 mN to 600 mN, which can be generated by another type of SMA coil, BMX200. The contraction and relaxation force rates of BMX200 are given by $D_{\text{on}} = D_{\text{off}} = 600$ mN/s. From simulations, we find that the height of the jump depends on the bending stiffness as plotted in Figure 9. At the original stiffness value, the robot cannot jump. Increasing the stiffness up to 0.0105 Nm/rad enables the robot to jump higher. Figure 10 shows the simulation result for a jump performed by a circular soft robot at $k_{\text{bend}} = 0.0105$ Nm/rad (see Extension 1). When the stiffness exceeds this threshold, the robot can hardly jump. Figure 11 shows the simulation result for a jump performed by a circular soft robot at $k_{\text{bend}} = 0.0107$ Nm/rad (see Extension 2). As shown in the figure, the robot deforms during the first and second time-steps, but cannot keep this deformed shape during the third step. This reduces the height of jumping. At $k_{\text{bend}} = 0.0125$ Nm/rad, the robot does not deform, causing the jump to fail. Thus, we need to select an appropriate bending stiffness for a successful jump.

4 Experimental Results using Circular Prototypes

The prototype of a circular soft robot shown in Figure 12, built to assess experimentally the feasibility of a deformable robot to crawl and jump, consists of eight BMX100 SMA coils, labeled A through H, attached to the inside of a circular rubber shell. The diameter of the circular body is 40 mm and the weight of the robot is 3.6 g. Each BMX100 coil is 20 mm long and consumes about 0.1 W. When voltage is applied to a coil, it contracts, causing the circular rubber to deform

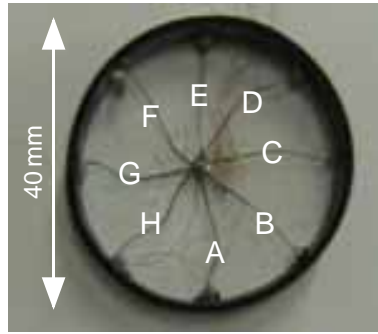


Figure 12: Prototype of a circular soft robot

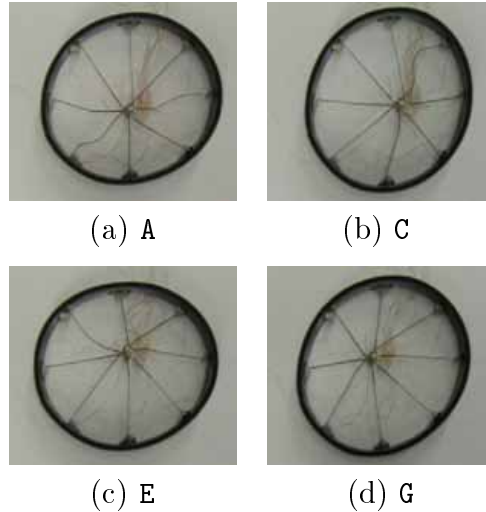


Figure 13: Deformation of a circular soft robot

as shown in Figure 13. Each figure corresponds to the deformation caused by the contraction of an individual coil A, C, E, or G.

4.1 Crawling

Figure 14 shows a sequence of snapshots of the prototype crawling. Voltage pattern BF is applied to the SMA coils. As shown in the figure, the circular robot can crawl on flat ground (see Extension 3).

Let us compare the simulation and experimental results for crawling. Figure 15 describes locomotion distances covered in 10 s at various step intervals. The prototype moves 260 mm in 10 s at a step interval of 0.6 s. That is, on average, the prototype moves about 65% of its diameter per second. As shown in the figure, simulation results agree with experimental results. Reducing the step interval within a certain range results in faster locomotion. Note that an activated SMA coil extends back to its natural length via natural radiation of heat, which limits the locomotion speed.

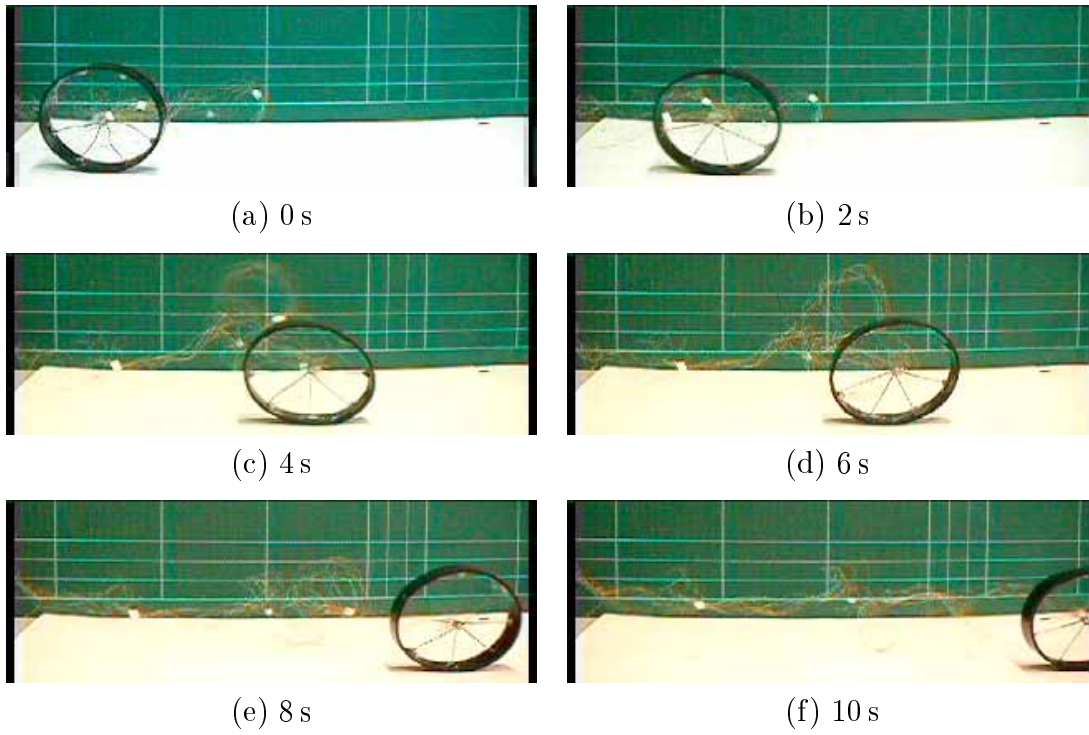


Figure 14: A crawling circular soft robot

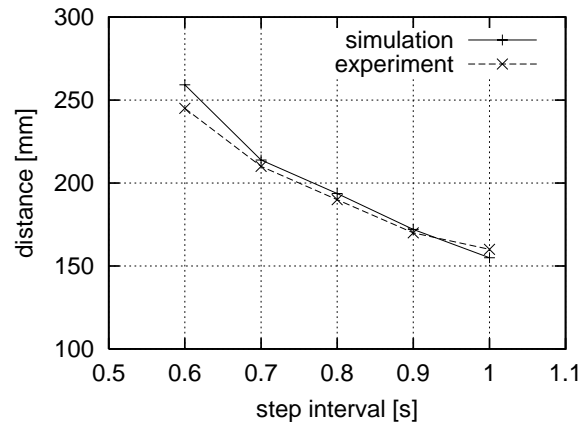


Figure 15: Comparison between simulation and experimental results for voltage pattern BF

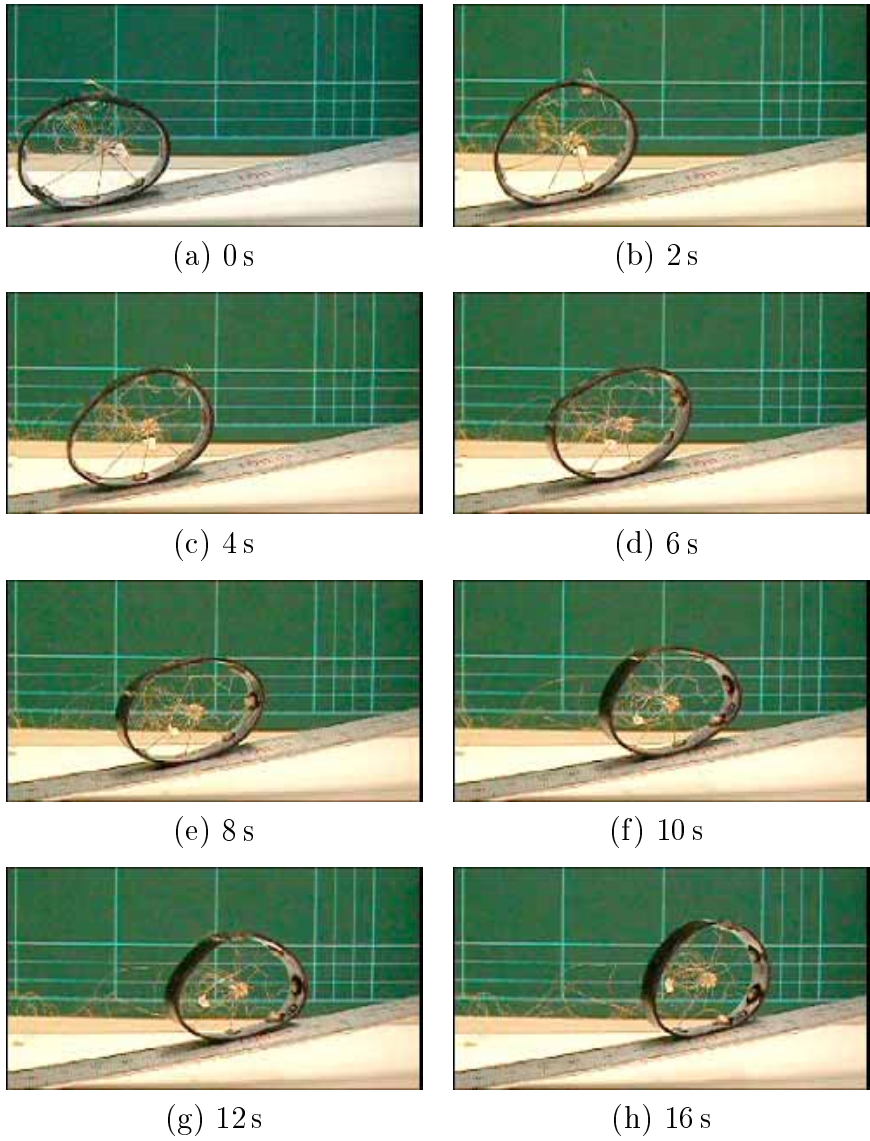


Figure 16: Circular soft robot climbing a slope

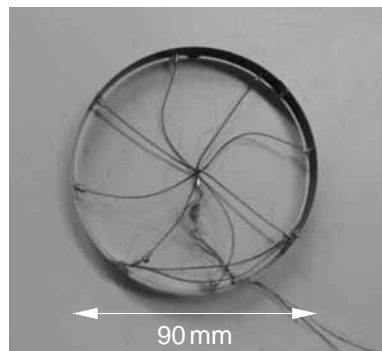


Figure 17: Prototype of a circular robot made of spring metal

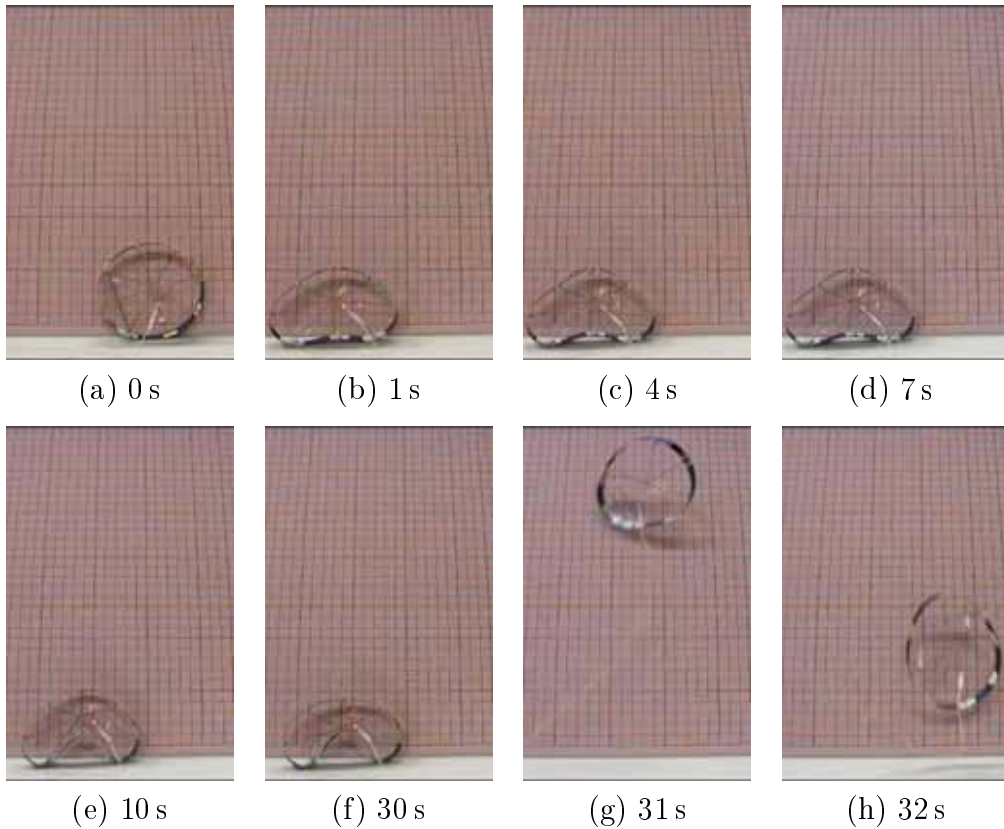


Figure 18: Circular soft robot jumping

4.2 Slope-climbing

Figure 16 shows a sequence of snapshots of the prototype climbing a slope. The prototype can climb up a 20° slope by applying pattern ABE (see Extension 4).

4.3 Jumping

SMA coil I is attached to a circular prototype for jumping. The voltage pattern illustrated in Figure 8 is applied to the set of SMA coils. Unfortunately, this prototype cannot jump on the ground. This implies that the rubber shell lacks bending elasticity or the SMA coils cannot generate sufficient force to deform the shell. As suggested in Section 3.3, we need to select an appropriate bending stiffness to realize a jump. The prototype shown in Figure 17 has a circular shell made of spring steel, to the inside of which are attached eight BMX200 SMA coils. The diameter of the circular body is 90 mm and the weight of the robot is 3 g. Each BMX200 coil is 45 mm long and consumes about $0.7W$. Figure 18 shows a sequence of snapshots of the spring steel prototype jumping when the voltage pattern illustrated in Figure 8 is applied. The jump height depends on the duration of each step. Let T_k be the k -th duration. Experiments show that when the durations are $T_1 = 4$ s, $T_2 = 3$ s, and $T_3 = 20$ s, the prototype can jump a distance of 160 mm, 1.8 times its diameter.

Another voltage pattern that produces a jump is illustrated in Figure 19. Before coil I is

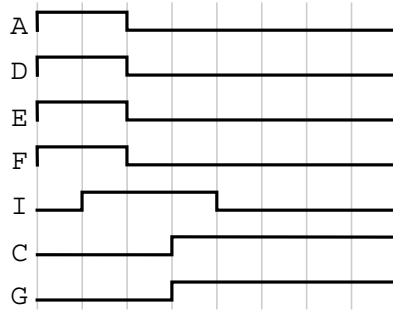


Figure 19: Voltage pattern for higher jumps

released, coils C and G are activated. This increases the curvature of the circular shell around the area of contact on the ground. The two coils remain activated, while coil I is released for jumping. Experiments show that durations of $T_1 = 4$ s, $T_2 = 3$ s, $T_3 = 15$ s, and $T_4 = 3$ s can make the prototype jump a distance of 300 mm (see Extension 5), which is more than 3 times its diameter, as shown in Figure 20.

5 Experimental Exploration to Three-dimensional Crawling and Jumping

Figure 21 shows a spherical soft prototype, designed in light of the observation in Section 4, that can crawl and jump three-dimensionally. The prototype consists of three orthogonally intersecting spring metal circular shells rather than a complete sphere because the latter would require a relatively large force to deform it. For crawling there are 18 BMX200 SMA coils and for jumping 4 BMX200 SMA coils attached to the inside of the circular shells. The diameter of the spherical body is 90 mm and the weight of the robot is 5 g. Each BMX200 coil is 45 mm long and consumes about $0.7W$. Figure 22 shows the attached SMA coils. Figure 22-(a), (b), and (c) show the top, side, and front view of the prototype, respectively. All the SMA coils used for crawling are illustrated in these figures. As can be seen in the figures, the SMA coils for crawling are attached between the center of the sphere and the three circular shells labeled C1, C2, and C3. Let us suppose that C1 lies on the x - y plane, as shown in Figure 22-(a). Two coils are along the x -axis from the center to the circular shell in the positive and negative directions, designated A100 and $A\bar{1}00$. The two coils along the y -axis are denoted by A010 and $A0\bar{1}0$. Four additional SMA coils, A110, $A1\bar{1}0$, $A10\bar{1}$, and $A10\bar{1}$, are attached to the circular shell. Coil A110 is located between A100 and A010. Note that coil A110 is described by the *digital sum* of A100 and A010. Thus, there are eight SMA coils involved in the circular shell C1. Circular shells C2 and C3 lie on the z - x and y - z planes, as shown in Figure 22-(b) and (c), respectively. The coils along the z -axis will be referred to as A001 and $A00\bar{1}$. Circular shells C2 and C3 also contain eight SMA coils, as illustrated in the figures. Thus, the 18 SMA coils used for crawling are labeled A100 and $A\bar{1}00$ through A001 and $A00\bar{1}$ as well as the digital sums of their adjacent pairs. Figure 22-(d) shows the bottom of the prototype. SMA coils for jumping are attached along a square formed by the terminal points of the four SMA coils for crawling, $A10\bar{1}$, $A01\bar{1}$, $A\bar{1}0\bar{1}$, and $A0\bar{1}\bar{1}$, which

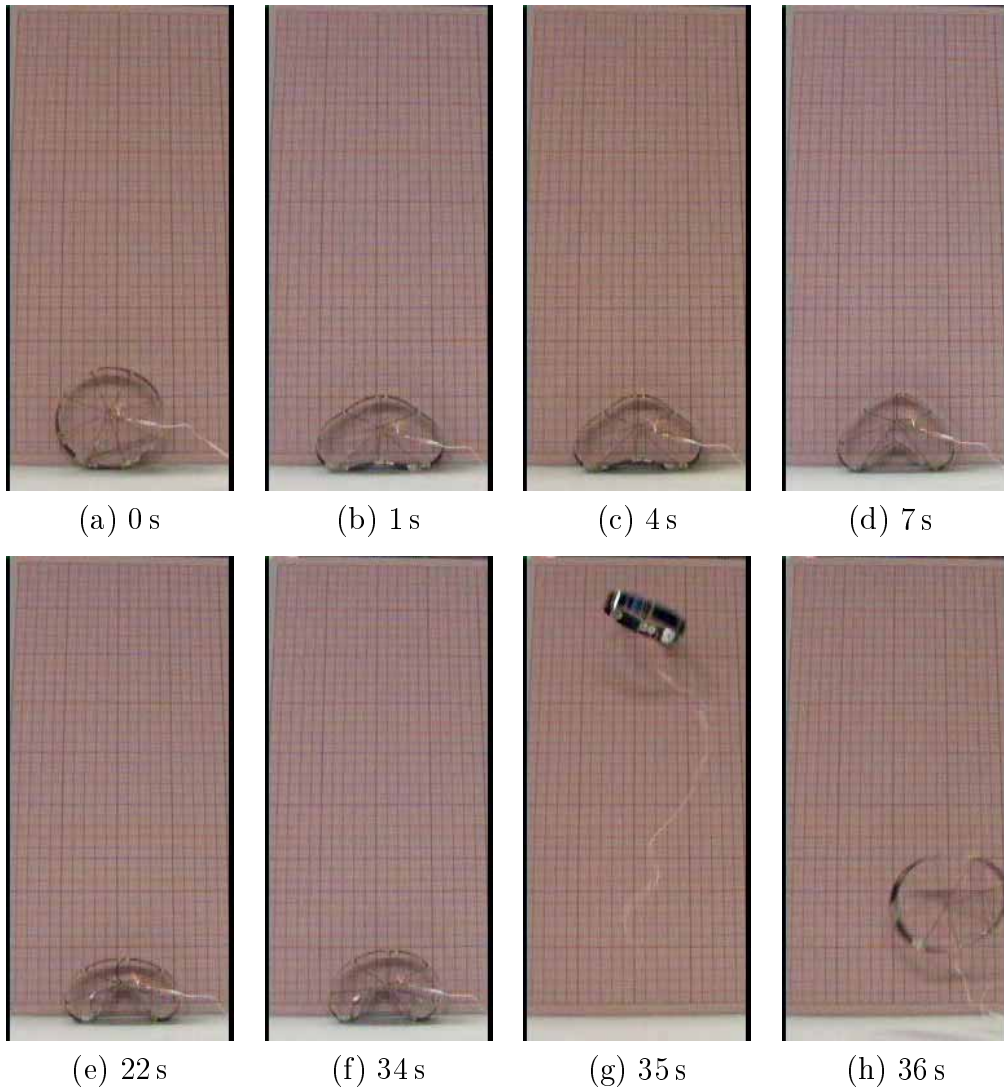


Figure 20: Circular soft robot jumping higher

neighbor $A00\bar{1}$. The SMA coils for jumping are labeled $B10\bar{1}$, $B01\bar{1}$, $B\bar{1}0\bar{1}$, and $B0\bar{1}\bar{1}$. Note that coil $B10\bar{1}$, for example, starts from the terminal point of $A10\bar{1}$, considering the rotation around $A00\bar{1}$ along the square.

5.1 Crawling

Our spherical prototype has eight stable orientations on the ground. This suggests that it can crawl through a sequence of transitions among the stable orientations. The three mutually orthogonal circular shells divide the sphere into eight spherical sectors. A stable orientation is then specified by the bottom spherical sector. Each spherical sector is labeled by the digital sum of the SMA coils attached to its three vertices. That is, the stable orientations are $S\bar{1}\bar{1}\bar{1}$, $S1\bar{1}\bar{1}$, $S\bar{1}1\bar{1}$, $S\bar{1}\bar{1}1$, $S11\bar{1}$, $S\bar{1}11$, $S1\bar{1}1$, and $S111$. Transition from one stable orientation to another can

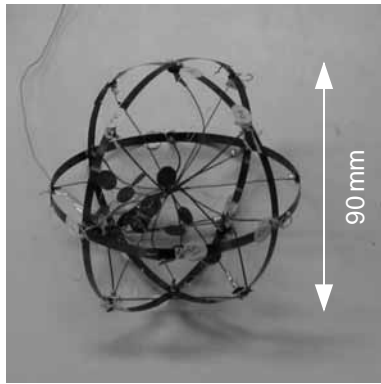


Figure 21: Prototype of a spherical soft robot

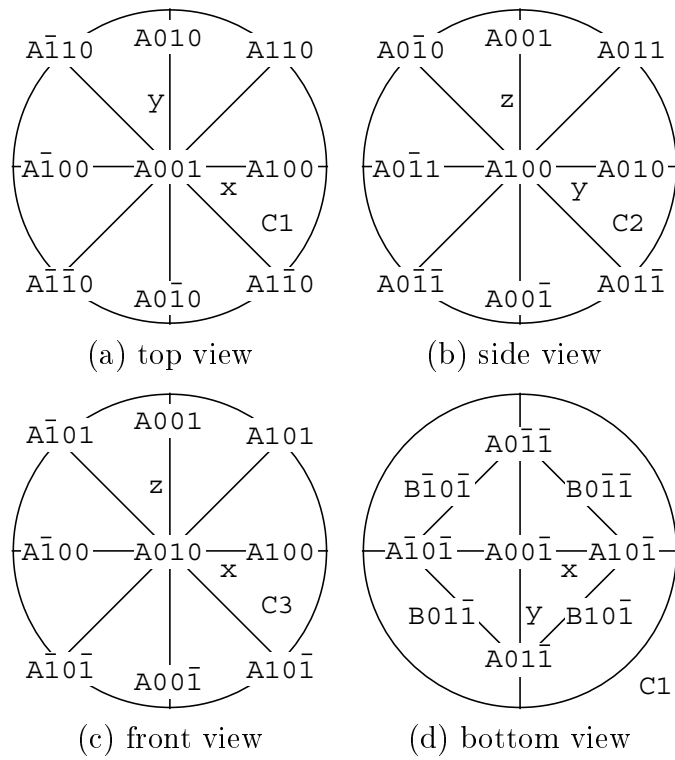


Figure 22: SMA coils attached to spherical prototype

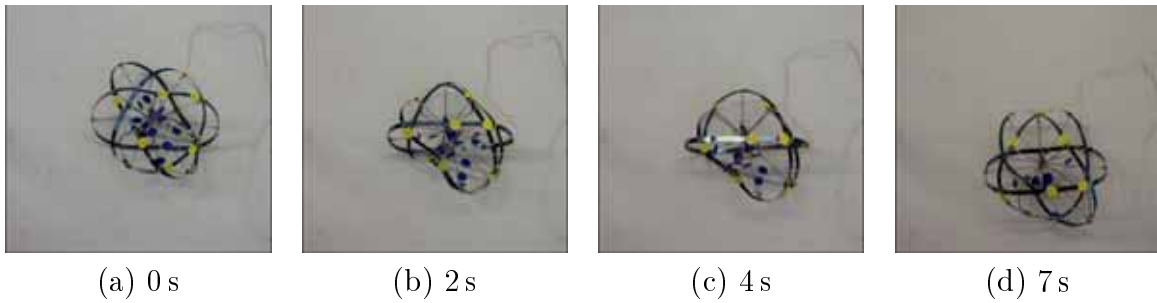


Figure 25: Spherical prototype crawling

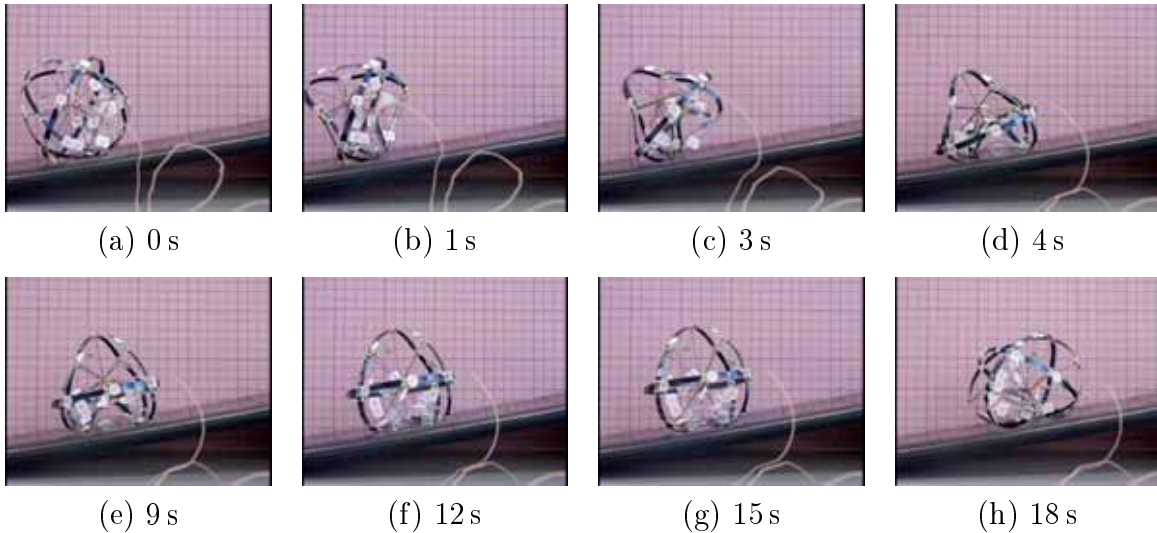


Figure 26: Spherical prototype climbing a slope

5.2 Slope-climbing

The spherical prototype can climb up a 6° slope through the voltage pattern 24-(a) and a 10° slope through the voltage pattern 24-(b) (see Extension 6). Figure 24-(b) describes the voltage pattern used to perform the transition from $S111$ to $S\bar{1}\bar{1}1$ via vertex $A001$. We have experimentally determined appropriate durations: $T_1 = 2$ s, $T_2 = 1$ s, $T_3 = 4$ s, $T_4 = 1$ s, $T_5 = 6$ s, and $T_6 = 10$ s. Figure 26 shows the snapshots of a climb of 10° slope.

5.3 Jumping

The voltage patterns shown in Figure 27 make the spherical prototype jump. Figures 27-(a) and (b) correspond to the voltage patterns given in Figures 8 and 19, respectively. Using the voltage patterns in Figures 27-(a) and (b), the prototype can jump 70 mm and 180 mm (i.e. twice its diameter), respectively. Figure 28 shows a sequence of snapshots of the spherical prototype higher jumping (see Extension 7).

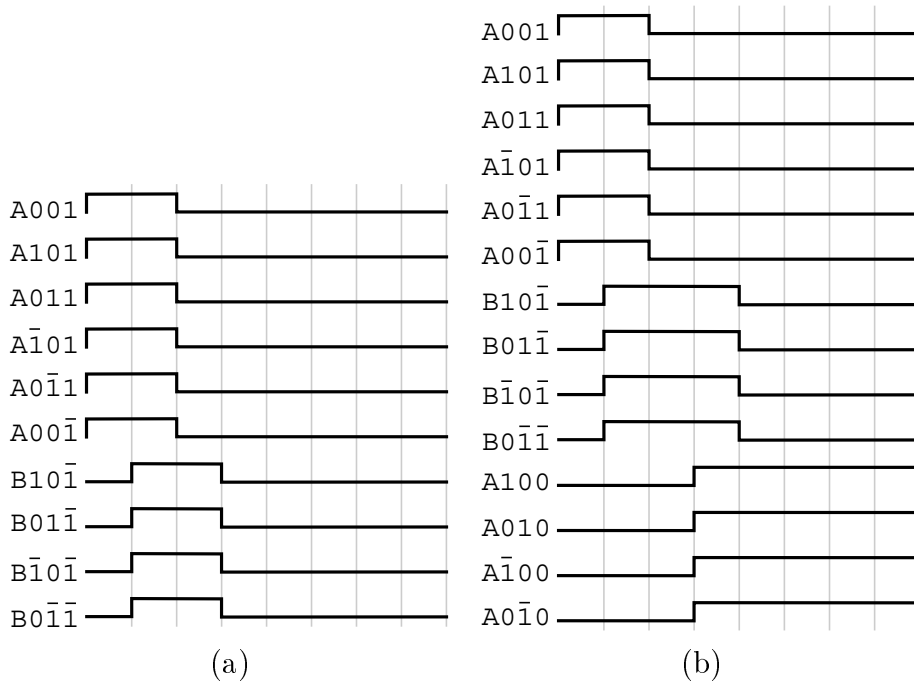


Figure 27: Voltage patterns for spherical prototype jumping

6 Concluding Remarks

In the present study, we developed a deformable robot capable of crawling and jumping. First, we described the principle of crawling and jumping using the deformation of the robot body. Second, in a physical simulation using a three-element model with a slider, we showed the feasibility of performing crawls and jumps with this robot. We applied particle-based modeling to simulate the behavior of a circular deformable robot. Through simulations, we found that the jump critically depends on the bend elasticity of the robot body. Next, we experimentally verified that a prototype of a circular soft robot can crawl and jump. The circular prototype moved about 65% of its diameter per second and climbed up a 20° slope. Another circular prototype jumped a distance over 3 times its diameter. Finally, we experimentally explored the crawling and jumping of a spherical soft robot.

Model parameters in a particle-based model depend not only on the shell's material but also on its geometry, making it difficult to model the behavior of deformable robots. We will apply differential geometry coordinates (Wakamatsu and Hirai 2004) to the model of a circular robot so that we can use material parameters, which are independent of the geometry, and analyze the bulking of the circular shell when the robot jumps. We will evaluate the potential and kinetic energies of the circular soft robot during crawling and jumping in order to get a better understanding of its behavior. Although soft actuators including SMA coils and polymer gel actuators show hysteresis in their deformation, which affects the performance of the robot, in the present model we have ignored it for simplification, but we intend to include it in a future model. Crawling depends on the gravitational potential energy and its temporal rate of change, which are determined by the dynamic deformation of the robot body. We will investigate theoretically

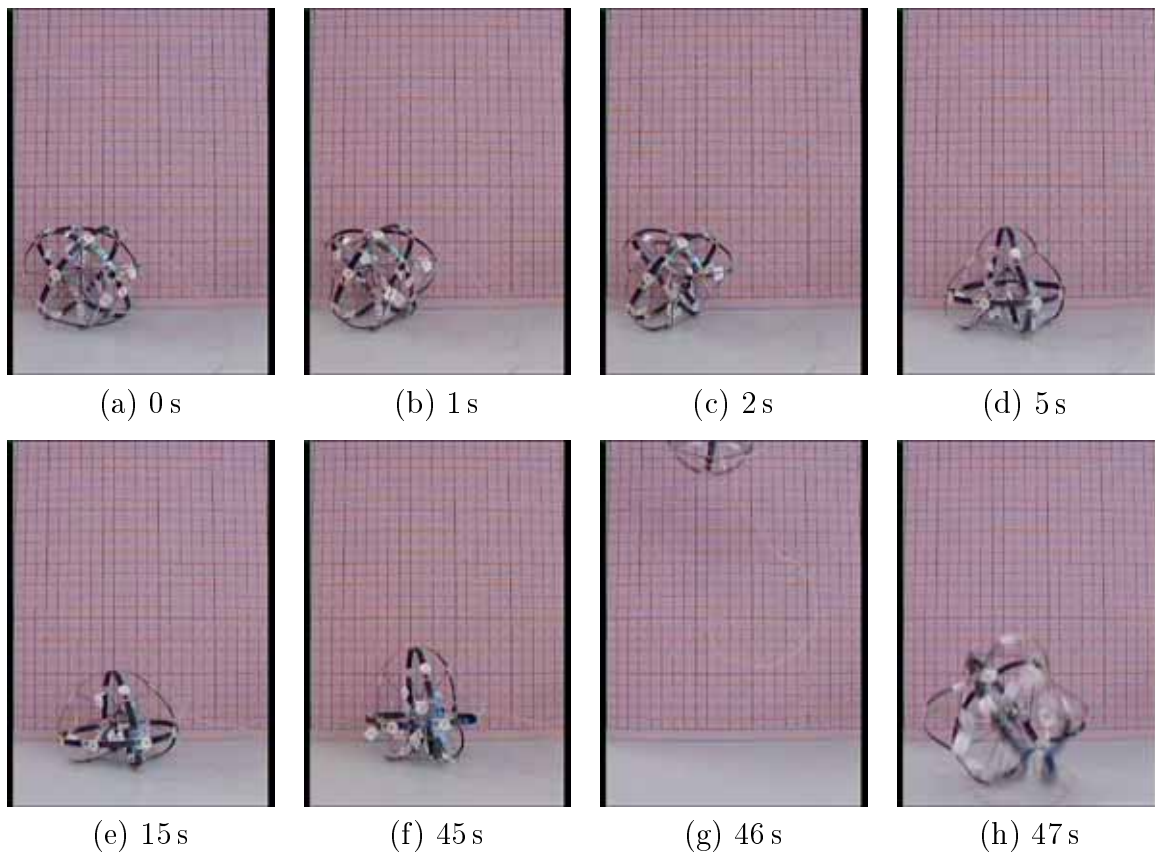


Figure 28: Spherical soft robot jumping

how the deformation characterizes crawling. We have shown the dependence of a jump on the elasticity of the robot body. We will also investigate how the jump depends on the viscosity of the robot body. It has been reported that a flea can jump about 100 times its length. We will investigate the mechanics of jumping through deformation to understand how deformation of a mechanical or biological system improves its performance. SMA coils consume too much power to be driven by on-board power sources. We will introduce polymer actuators to build self-supporting robots that crawl and jump.

Acknowledgment

This research was supported in part by the NEDO 21st Century Robot Challenge Program, Japan.

Appendix: Index to Multimedia Extensions

The multimedia extensions to this article are at <http://www.ijrr.org>.

Table of Multimedia Extensions

| Extension | Type | Description |
|-----------|-------|---|
| 1 | Video | JumpingSimulation0105.mpg. Simulation of a circular soft robot jumping at bending elasticity $k_{\text{bend}} = 0.0105 \text{ Nm/rad}$. |
| 2 | Video | JumpingSimulation0107.mpg. Simulation of a circular soft robot jumping at bending elasticity $k_{\text{bend}} = 0.0107 \text{ Nm/rad}$. |
| 3 | Video | CircularRobotCrawling.mpg. A circular soft robot crawling on flat ground. |
| 4 | Video | CircularRobotSlopeClimbing.mpg. A circular soft robot climbing a 20° slope. |
| 5 | Video | CircularRobotJumping.mpg. A circular soft robot jumping. |
| 6 | Video | SphericalRobotSlopeClimbing.mpg. A spherical soft robot climbing a 10° slope. |
| 7 | Video | SphericalRobotJumping.mpg. A spherical soft robot jumping. |

References

- Ashley, S. 2003. *Artificial Muscles*, Scientific American, October, pp.34–41.
- Book, W. J. and Majette, M. 1983. *Controller Design for Flexible, Distributed Parameter Mechanical Arms Via Combined State Space and Frequency Domain Techniques*, Trans. ASME, J. Dynamic Systems, Measurement, and Control, Vol.105, December, pp.245–254.
- Chen, I.-M., Li, H.-S., and Cathala, A. 2003. *Mechatronic Design and Amoebot – A Metamorphic Underwater Vehicle*, Journal of Robotic Systems, Vol.20, No.6, pp.307–314.
- Choi, H. R., Jung, K. M., Kwak, J. W., Lee, S. W., Kim, H. M., Jeon, J. W., and Nam, J. D. 2003. *Digital Polymer Motor for Robotic Applications*, Proc. IEEE Int. Conf. on Control Applications, Taipei, September, pp.1857–1862.
- Ge, S. S., Lee, T. H., and Zhu, G. 1996. Improving Joint PD Control of Single-link Flexible Robots by Strain/Tip Feedback, Proc. IEEE Int. Conf. on Control Applications, Dearborn, September, pp.965–969.
- Hale, E., Schara, N., Burdick, J., and Fiorini, P. 2000. *A Minimally Actuated Hopping Rover for Exploration of Celestial Bodies*, Proc. IEEE Int. Conf. on Robotics and Automation, San Francisco, April, pp.420–427.
- Higashimori, M., Harada, M., Yuya, M., Ishii, I., and Kaneko, M. 2005. *Dimensional Analysis Based Design on Tracing Type Legged Robots*, Proc. IEEE Int. Conf. on Robotics and Automation, pp.3744–3749, Barcelona, April.
- Hirai, T., Uddin, Z., Zheng, J., Yamaguchi, M., Kobayashi, S., Watanabe, M., and Shirai, H. 2003. *Quick and large electrostrictive deformation of non-ionic soft polymer materials*, Smart Structures and Materials 2003, Proc. SPIE, Vol. 5051, pp.198–206.
- Hirose, S. and Morishima, A. 1990. *Design and Control of a Mobile Robot with an Articulated Body*, Int. J. of Robotics Research, Vol. 9, No. 2, pp.99–114.

- Hirose, S. 1993. *Biologically Inspired Robots: Snake-like Locomotors and Manipulators*, Oxford University Press.
- Hodgins, J. K. and Raibert, M. H. 1990. *Biped Gymnastics*, Int. J. of Robotics Research, Vol. 9, No. 2, pp.115–132.
- Kaneko, M., Takenaka, R., Higashimori, M., Namiki, A., and Ishikawa, M. 2003. *The 100G Capturing Robot –Too Fast to See*, IEEE Trans. on Mechatronics, Vol. 8, No. 1, pp.37–44.
- Kimura, M., Sugiyama, Y., Tomokuni, S., and Hirai, S. 2003. *Constructing Rheologically Deformable Virtual Objects*, Proc. IEEE Int. Conf. on Robotics and Automation, Taipei, September, pp.3237–3243.
- Matsuno, F., Ohno, T., and Orlov, Y. V. 2002. *Proportional Derivative and Strain (PDS) Boundary Feedback Control of a Flexible Space Structure with a Closed-Loop Chain Mechanism*, Automatica, 38(7), pp.1201–1211.
- Nguyen, P. and Arimoto, S. 2001. *Performance of Pinching Motions of Two Multi-DOF Robotic Fingers with Soft-Tips*, Proc. IEEE Int. Conf. on Robotics and Automation, Seoul, May, pp.2344–2349.
- Otake, M., Kagami, Y., Inaba, M., and Inoue, H. 2002. *Motion design of a starfish-shaped gel robots made of electroactive polymer gel*, Robotics and Autonomous Systems, Vol. 40, pp.185–191.
- Pelrine, R., Kornbluh, R., Pei, Q., and Joseph, J. 2000. *High-speed Electrically Actuated Elastomers with Strain Greater Than 100%*, Science, Vol. 287, February, pp.836–839.
- Raibert, M. H. 1986. *Legged Robots that Balance*, The MIT Press, Cambridge.
- Rothschild, M., Schlein, Y., and Ito, S. 1986. *A Colour Atlas of Insect Tissues via the Flea*, p.86, *The jumping flea*, Wolfe Publishing.
- Saranli, U., Buehler, M., and Koditschek, D. E. 2001. *RHex: A Simple and Highly Mobile Hexapod Robot*, Int. J. of Robotics Research, Vol. 20, No. 7, pp.616–631.
- Selden, B., Cho, K.-J., and Asada, H.-H. 2004. *Segmented Binary Control of Shape Memory Alloy Actuator Systems Using the Peltier Effect*, Proc. IEEE Int. Conf. on Control Applications, New Orleans, April, pp.4931–4936.
- Shimoga, K. B. and Goldenberg, A. A. 1996. *Soft Robotic Fingertips Part II: Modeling and Impedance Regulation*, Int. J. of Robotics Research, Vol.15, No.4, pp.335–350.
- Sodaplay. <http://www.sodaplay.com>.
- Wakamatsu, H. and Hirai, S. 2004. *Static Modeling of Linear Object Deformation based on Differential Geometry*, Int. J. of Robotics Research, Vol. 23, No. 3, March, pp.293–311.
- Xydas, N. and Kao, I. 1999. *Modeling of Contact Mechanics and Friction Limit Surfaces for Soft Fingers in Robotics, with Experimental Results*, Int. J. of Robotics Research, Vol.18, No.8, pp.941–950.
- Yim, M., Eldershaw, C., Zhang, Y., and Duff, D. 2004. *Limbless Conforming Gaits with Modular Robots*, Proc. Int. Symp. on Experimental Robotics, Singapore, June.